Braz J Phys (2015) 45:399–403
DOI 10.1007/s13538-015-0341-z

SOCIEDADE BRASILEIRA DE FÍSICA

CONDENSED MATTER

Structural, Mechanical, and Electronic Properties of Monoclinic $N_2H_5N_3$ Under Pressure

Qi-Jun Liu[1,2] · **Fu-Sheng Liu**[1,2] · **Zheng-Tang Liu**[3]

Received: 26 March 2015 / Published online: 10 June 2015

Abstract Structural, elastic, mechanical, and electronic properties of monoclinic $N_2H_5N_3$ at zero and high pressure have been investigated using the plane-wave ultrasoft pseudopotential method within the density-functional theory (DFT). The pressure dependences of structural parameters, elastic constants, mechanical properties, band gaps, and density of states of monoclinic $N_2H_5N_3$ have been calculated and discussed. The obtained results show that monoclinic $N_2H_5N_3$ is unstable at pressures exceeding the value 126.1 GPa. The ratio of B/G and the Cauchy's pressure indicate that monoclinic $N_2H_5N_3$ behaves in ductile nature with pressure ranging from 0 to 200 GPa.

Keywords Density-functional theory · Mechanical properties · Pressure · Monoclinic $N_2H_5N_3$

1 Introduction

$N_2H_5N_3$ is of great interest due to its potential as high energy density material (HEDM). HEDMs have been widely investigated because of their excellent properties compared with those of conventional energetic materials such as large energy release, good thermal stability, and excellent detonation velocities [1–4]. Nitrogen-rich compounds are promising HEDMs [5, 6], which attract our attention. Among them, $N_2H_5N_3$ with high nitrogen content shows potential for HEDMs because of its strong bonds including plentiful energies between nitrogen atoms [7]. Monoclinic $N_2H_5N_3$ with $P2_1/b$ space group has N_3^- and $N_2H_5^+$ ions [8], which has been studied by first-principles density-functional theory [7]. However, its fundamental properties under high-pressure are still lacking. High-pressure is an important condition for practical applications of HEDMs such as future fuel in advanced propulsion systems and inertial confinement fusion research [9, 10]. Moreover, there is much interest in the potential application of explosives. As we know, the structure and behavior of explosives under extreme conditions are important to give valuable information of their sensitivity, performance, and safety [11]. Hence, in order to obtain a thorough knowledge of this compound under pressure, we investigate the monoclinic $N_2H_5N_3$ with pressure ranging from 0 to 200 GPa by density-functional theory.

2 Computational Details

Our calculations were performed using the plane-wave ultrasoft pseudopotential method as implemented in CASTEP code [12]. The exchange-correlation interaction is in the form of generalized gradient approximation (GGA) with Perdew-Burke-Ernzerholf (PBE) function [13]. Moreover, the TS scheme [14] is employed to improve the accuracy of the calculations. The cutoff energy

✉ Qi-Jun Liu
qijunliu@home.swjtu.edu.cn

[1] School of Physical Science and Technology, Southwest Jiaotong University, Key Laboratory of Advanced Technologies of Materials, Ministry of Education of China, Chengdu 610031, People's Republic of China

[2] Bond and Band Engineering Group, Sichuan Provincial Key Laboratory (for Universities) of High Pressure Science and Technology, Southwest Jiaotong University, Chengdu 610031, People's Republic of China

[3] State Key Laboratory of Solidification Processing, School of Materials Science and Engineering, Northwestern Polytechnical University, Xi'an 710072, People's Republic of China

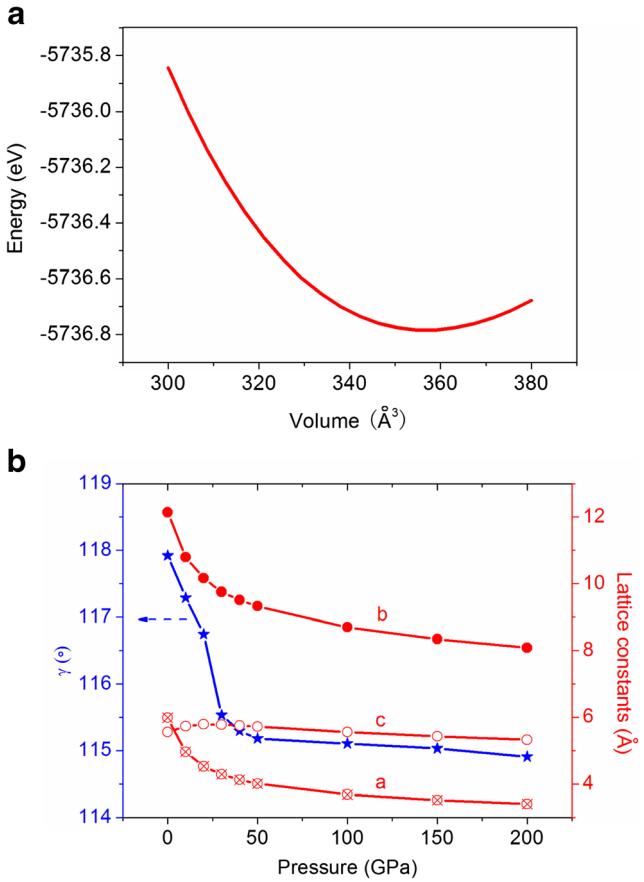

Fig. 1 **a** Calculated energy versus volume for $N_2H_5N_3$; **b** pressure dependences of structural parameters *a*, *b*, *c*, and γ at zero temperature and pressure up to 200 GPa

of the plane-wave expansion is 600 eV and the H $1s^1$ and N $2s^22p^3$ electrons are treated as valence electrons. The self-consistent convergence of total energy is 5.0×10^{-6} eV/atom, maximum force within 0.01 eV/Å, maximum displacement within 5×10^{-4} Å, and maximum stress within 0.02 GPa.

3 Results and Discussion

3.1 Structural Properties

The crystal packing of the potential explosive has an influence on its performance and sensitivity. Hence, we firstly optimize its structural parameters. $N_2H_5N_3$ is a monoclinic structure with the structural parameters a=5.663(2) Å, b=12.436(3) Å, c=5.506(2) Å, and γ=114.0(1)° [8]. Our calculations result in the following structural parameters: a=5.9846 Å, b=12.1388 Å, c=5.5580 Å, and γ=117.921°. We find that these parameters a, c, and γ are overestimated, but b is underestimated. The calculated volume of a unit cell is 356.766 Å^3 at 0 GPa and 0 K, which is consistent with the experimental value [8] within 0.73 % (overestimation). The equation of state is obtained by using the third-order Birch-Murnaghan equation [15]:

$$E(V)=E_0+\frac{9V_0B_0}{16}\left\{\left[\left(\frac{V_0}{V}\right)^{2/3}-1\right]^3B'+\left[\left(\frac{V_0}{V}\right)^{2/3}-1\right]^2\left[6-4\left(\frac{V_0}{V}\right)^{2/3}\right]\right\} \quad (1)$$

where E_0 and V_0 are associated with the values at zero pressure. The optimization plot is shown in Fig. 1a. We obtain the bulk modulus B_0 (B_{EOS}) and the pressure derivative of bulk modulus (B') at zero pressure (B_0=24.0 GPa and B'=5.1). The value of B_0 is consistent with the datum obtained from the elastic constants (23.9 GPa).

In Fig. 1b, we illustrate the pressure dependences of structural parameters *a*, *b*, *c*, and γ at zero temperature and pressure up to 200 GPa. To the best of our knowledge, no such research of this compound has been studied to date. However, our structural parameters under zero pressure are in good agreement with the experimental data, indicating the repeatability and accuracy of the present methods, which can be used to

Table 1 Calculated elastic constants C_{ij} (GPa), bulk modulus B (GPa), shear modulus G (GPa), Young's modulus E (GPa), B/G, Poisson's ratio ν, Lamé's constants μ, and λ (GPa) of monoclinic $N_2H_5N_3$ under pressure

	C_{11}	C_{12}	C_{13}	C_{15}	C_{22}	C_{23}	C_{25}	C_{33}	C_{35}	C_{44}	C_{46}	C_{55}	C_{66}	B	G(μ)	E	B/G	ν	λ
0	28.4	16.6	21.6	−1.3	29.1	19.8	1.4	54.5	1.6	10.7	−0.8	11.7	8.0	23.9	9.2	24.5	2.598	0.329	17.8
10	66.0	37.3	62.7	−4.6	83.7	74.4	0.9	153.7	0.7	23.0	−0.2	36.4	26.0	62.6	24.2	64.3	2.587	0.329	46.5
20	109.6	67.3	89.8	−3.4	137.0	111.8	−0.3	240.1	−1.2	51.0	1.7	68.6	41.1	103.6	43.8	115.2	2.365	0.315	74.4
30	150.7	87.3	114.1	−7.5	184.9	134.7	−0.1	306.0	0.2	78.5	0.4	90.8	53.9	135.7	61.5	160.3	2.207	0.303	94.7
40	209.2	115.9	146.0	−5.6	233.4	167.2	−0.5	365.4	3.1	103.0	−3.0	119.5	64.6	176.1	78.3	204.6	2.249	0.306	124.0
50	254.6	142.3	160.7	−8.8	289.8	195.5	0.0	451.9	−0.1	123.4	−5.5	142.5	83.8	212.2	98.3	255.5	2.159	0.299	146.6
100	501.0	272.9	275.6	−7.9	520.4	361.7	0.0	711.0	0.3	222.8	−19.5	249.5	157.3	387.0	172.4	450.3	2.245	0.306	272.1
150	722.7	383.8	379.8	−3.6	726.0	496.0	−0.1	893.4	−0.9	314.7	−32.4	335.5	230.7	534.8	236.8	619.0	2.258	0.307	377.0
200	936.3	505.7	470.2	−0.9	887.0	672.8	−0.2	1148.0	−0.2	397.5	−50.2	399.4	313.7	689.2	290.8	764.8	2.370	0.315	495.3

study this compound under pressure. It is easy to note that these parameters a, b, and γ decrease with increase of the pressure, namely the parameters a, b, and γ nonlinearly decrease monotonously with pressure up to 50 GPa, and linearly decrease monotonously with pressure up to 200 GPa. However, lattice constant c increases with pressure from 0 to 20 GPa and decreases with pressure from 30 to 200 GPa. Hence, there is a peak value of c between 20 and 30 GPa. Moreover, it varies slowly, showing that the resistance along the c-axis is larger than that along a-/b-axis.

3.2 Elastic and Mechanical Properties

Monoclinic structure has a low symmetry and there are 13 independent elastic constants for this structure. The calculated elastic constants of monoclinic $N_2H_5N_3$ under pressure are presented in Table 1, which are depicted in Fig. 2 to be clear at a glance. The elastic constants almost change linearly when pressure increases. Specially, except C_{15}, C_{25}, C_{35}, and C_{46}, the others increase monotonously with increase of the pressure. Moreover, the C_{33} increases rapidly, indicating that it is more sensitive to pressure than that of the others. For monoclinic structure, the mechanical stability criteria under pressure are [16–18]:

$$\begin{gathered}(C_{11}-P)>0,\ (C_{22}-P)>0,\ (C_{33}-P)>0,\ (C_{44}-P)>0,\ (C_{55}-P)>0,\\ (C_{66}-P)>0,\ (C_{11}+C_{22}+C_{33}+2C_{12}+2C_{13}+2C_{23}+3P)>0\\ (C_{33}-P)(C_{55}-P)>C_{35}^2,\ \ (C_{44}-P)(C_{66}-P)>C_{46}^2\end{gathered} \tag{2}$$

$$(C_{22}+C_{33})>(2C_{23}+4P) \tag{3}$$

$$\begin{gathered}\left\{(C_{22}-P)\left[(C_{33}-P)(C_{55}-P)-C_{35}^2\right]+2(C_{23}+P)C_{25}C_{35}\right\}\\ >\left[(C_{23}+P)^2(C_{55}-P)+C_{25}^2(C_{33}-P)\right]\end{gathered} \tag{4}$$

$$\begin{gathered}\left\{\begin{array}{l}2\,C_{15}C_{25}[(C_{33}-P)(C_{12}+P)-(C_{13}+P)(C_{23}+P)]\\ +2C_{15}C_{35}[(C_{22}-P)(C_{13}+P)-(C_{12}+P)(C_{23}+P)]\\ +2C_{25}C_{35}[(C_{11}-P)(C_{23}+P)-(C_{12}+P)(C_{13}+P)]\\ +\ \ (C_{55}-P)\ \ (C_{11}-P)\ \ (C_{22}-P)\ \ (C_{33}-P)\\ +\ 2\ \ (C_{55}-P)\ \ (C_{12}+P)\ \ (C_{13}+P)\ \ (C_{23}+P)\end{array}\right\}\\ >\left\{\begin{array}{l}C_{15}^2\left[(C_{22}-P)(C_{33}-P)-(C_{23}+P)^2\right]\\ +C_{25}^2\left[(C_{11}-P)(C_{33}-P)-(C_{13}+P)^2\right]\\ +C_{35}^2\left[(C_{11}-P)(C_{22}-P)-(C_{12}+P)^2\right]\\ +\ (C_{55}-P)\ \ (C_{11}-P)\ \ (C_{23}+P)^2\\ +\ (C_{55}-P)\ \ (C_{22}-P)\ \ (C_{13}+P)^2\\ +\ (C_{55}-P)\ \ (C_{33}-P)\ \ (C_{12}+P)^2\end{array}\right\}\end{gathered} \tag{5}$$

According to our calculated elastic constants, we note that these constants satisfy the stability condition (2) with pressure up to 200 GPa. However, the stability conditions (3), (4), and (5) are not satisfied when pressure increases up to 159.6, 154.3, and 126.1 GPa, respectively, which are shown in Fig. 3. We can conclude that monoclinic $N_2H_5N_3$ is not mechanically stable at the pressure of 126.1 GPa.

Table 1 shows the bulk modulus, shear modulus, Young's modulus, B/G, Poisson's ratio, and Lamé's constants of monoclinic $N_2H_5N_3$ under pressure, which are obtained by [19–21]:

$$B_{Hill}=\frac{1}{2}\left(\frac{1}{S_{11}+S_{22}+S_{33}+2S_{12}+2S_{13}+2S_{23}}+\frac{C_{11}+C_{22}+C_{33}+2C_{12}+2C_{13}+2C_{23}}{9}\right) \tag{6}$$

$$G_{Hill}=\frac{1}{2}\left(\begin{array}{c}\dfrac{15}{4S_{11}+4S_{22}+4S_{33}-4S_{12}-4S_{13}-4S_{23}+3S_{44}+3S_{55}+3S_{66}}\\ +\dfrac{C_{11}+C_{22}+C_{33}-C_{12}-C_{13}-C_{23}+3C_{44}+3C_{55}+3C_{66}}{15}\end{array}\right) \tag{7}$$

$$E_{Hill}=\frac{9B_{Hill}G_{Hill}}{G_{Hill}+3B_{Hill}} \tag{8}$$

$$\nu_{Hill}=\frac{1}{2}\left[\frac{B_{Hill}-(2/3)G_{Hill}}{B_{Hill}+(1/3)G_{Hill}}\right] \tag{9}$$

$$\mu_{Hill}=E_{Hill}/[2(1+\nu_{Hill})] \tag{10}$$

$$\lambda_{Hill}=\nu_{Hill}E_{Hill}/[(1+\nu_{Hill})(1-2\nu_{Hill})] \tag{11}$$

where the S_{ij} is elastic compliance constants.

These values are shown in Fig. 4. We can see that bulk modulus, shear modulus, Young's modulus, and Lamé's constants linearly increase monotonously when pressure increases, indicating that the resistances to uniaxial tension, fracture, and plastic deformation are enhanced. Moreover, the increase of resistance to plastic deformation is lowest due to the most slow increase of shear modulus, the increase of resistance to uniaxial tension is maximal due to the most quick increase of Young's modulus. The B/G and Poisson's ratio have similar variations shown in Fig. 4b. They decrease with increase of the pressure, and reach the minimum under

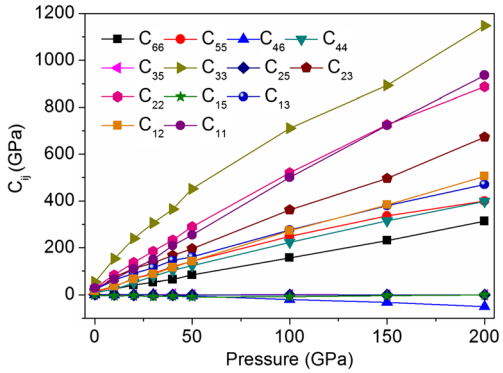

Fig. 2 Elastic constants of monoclinic $N_2H_5N_3$ under pressure

50 GPa. Then, they increase with the pressure. According to Pugh's supposition [22], the critical value 1.75 of B/G can be used to separate ductile and brittle materials, namely B/G >1.75 means that the material behaves in a ductile manner. We can see that monoclinic $N_2H_5N_3$ shows ductile behavior with pressure ranging from 0 to 200 GPa. The ductility decreases with increase of the pressure, and becomes the worst under 50 GPa, whereafter it is enhanced. The ductility of monoclinic $N_2H_5N_3$ can be further proved by the Cauchy's pressure (C_{12}–C_{44}) [23]. The positive and negative values of the parameter C_{12}–C_{44} indicate that the material exhibits ductile and brittle properties, respectively. According to our data presented in Table 1, this parameter is positive in the whole examined range of the pressure variation, 0–200 GPa, indicating the ductility of monoclinic $N_2H_5N_3$.

3.3 Electronic Properties

Figure 5 displays the band gaps of monoclinic $N_2H_5N_3$ at different pressures. At zero pressure, an indirect band gap of 3.975 eV from the top valence band at D point to the bottom conduction band at Γ point occurs. However, with pressure ranging from 10 to 100 GPa, a direct band gap for monoclinic $N_2H_5N_3$ appears at Γ point. Then, an indirect band gap from D point to Z point appears again. In Fig. 5a, it is clear that the

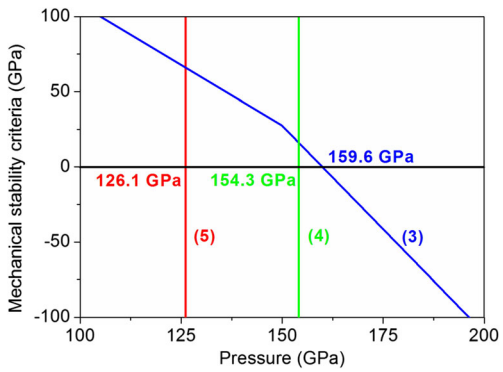

Fig. 3 Mechanical stability versus pressure for monoclinic $N_2H_5N_3$

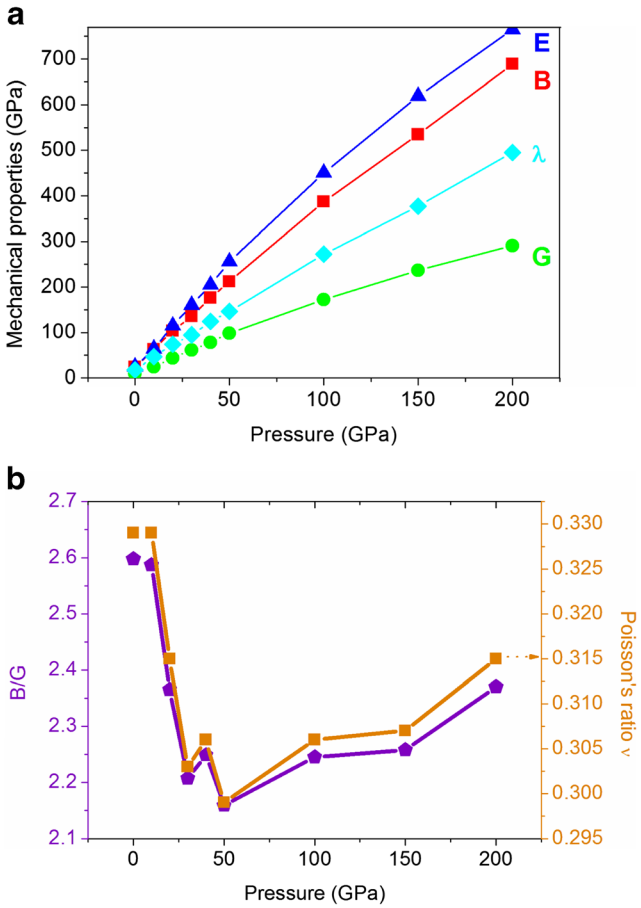

Fig. 4 Mechanical properties versus pressure for monoclinic $N_2H_5N_3$: **a** bulk modulus, shear modulus, Young's modulus, and Lamé's constants; **b** B/G and Poisson's ratio

decreases of the indirect band gaps are observed with increase of the pressure. For energetic materials with similar structure/similar thermal decomposition mechanism, it is known that they decompose and explode easily when the band gaps become small due to the effortless electron transfers from valence bands to conduction bands [24]. Hence, the impact sensitivity of monoclinic $N_2H_5N_3$ is sensitive with increase of the pressure. How about the direct band gaps with the pressure? In Fig. 5b, we can see that the direct band gaps at Z, Γ, B, D, E, and C points decrease with the increase of the pressure. The direct band gaps at Y and A points increase with pressure from 0 to 30 GPa, then they decrease with the increase of the pressure. In order to get more electronic nature of monoclinic $N_2H_5N_3$ under pressure, a plot of total density of states is shown in Fig. 6. When the pressure is applied, the narrowed energy gaps appear due to the shift of the conduction band to lower energy levels.

4 Conclusions

The first-principle calculations have been performed to investigate the structural, elastic, mechanical, and electronic

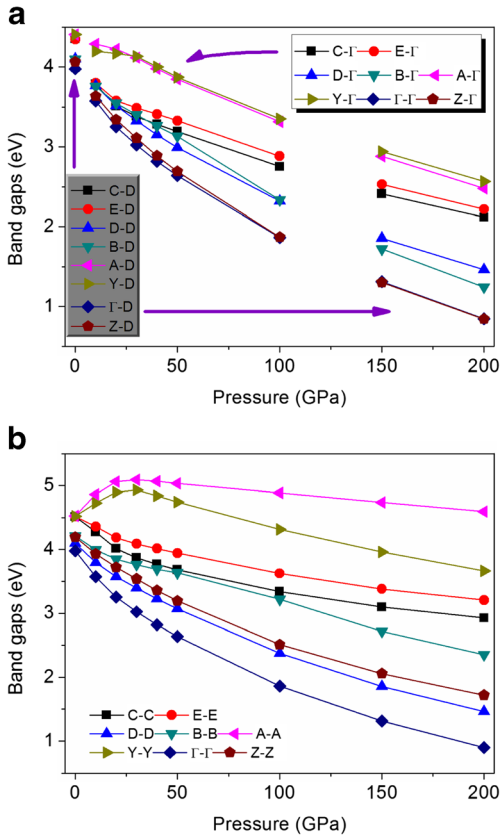

Fig. 5 Pressure dependences of the indirect (**a**) and direct (**b**) band gaps of monoclinic $N_2H_5N_3$

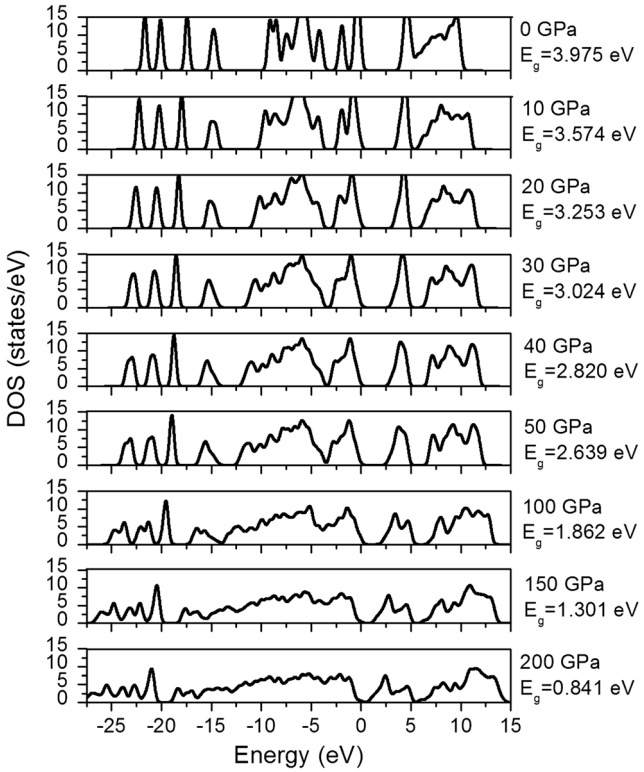

Fig. 6 Density of states versus pressure of monoclinic $N_2H_5N_3$

properties of monoclinic $N_2H_5N_3$ under pressure. Our calculated structural parameters under zero pressure are in agreement with the experimental values. We have obtained elastic constants and mechanical properties with pressure ranging from 0 to 200 GPa. To the best of our knowledge, there is no data of monoclinic $N_2H_5N_3$ under pressure to compare. This material is mechanically stable up to 126.1 GPa and shows ductile nature. In general, the explosives may react under extreme conditions, so we hope these data can help to offer a theoretical basis for the applications of monoclinic $N_2H_5N_3$.

Acknowledgments This work was supported by the National Basic Research Program of China (Grant No. 2011CB808201), the National Natural Science Foundation of China (Grant No. 51402244), the Fundamental Research Fund for the Central Universities, China (Grant Nos. 2682014CX084 and 2682014ZT31), and the fund of the State Key Laboratory of Solidification Processing in NWPU (Grant No. SKLSP201511).

References

1. G.X. Wang, X.D. Gong, Y. Liu, H.C. Du, X.J. Xu, H.M. Xiao, J. Hazard. Mater. **177**, 703–710 (2010)
2. W.G. Xu, X.F. Liu, S.X. Lu, J. Mol, Struct.: THEOCHEM **864**, 80–84 (2008)
3. D.B. Lempert, G.N. Nechiporenko, S.I. Soglasnova, Combust. Expl. Shock Waves **45**, 160–168 (2009)
4. Y. Pan, W.H. Zhu, H.M. Xiao, Comput. Theor. Chem. **1019**, 116–124 (2013)
5. Y. Pan, J.S. Li, B.B. Cheng, W.H. Zhu, H.M. Xiao, Comput. Theor. Chem. **992**, 110–119 (2012)
6. C.C. Zhang, W.H. Zhu, H.M. Xiao, Comput. Theor. Chem. **967**, 257–264 (2011)
7. Q.J. Liu, W. Zeng, F.S. Liu, Z.T. Liu, Comput. Theor. Chem. **1014**, 37–42 (2013)
8. G. Chiglien, J. Etienne, S. Jaulmes, P. Laruelle, Acta Crystallogr. **B30**, 2229–2233 (1974)
9. R.C. Striebich, J. Lawrence, J. Anal. Appl. Pyrolysis **70**, 339–352 (2003)
10. D.H.H. Hoffmann, A. Blazevic, P. Ni, O. Rosmej, M. Roth, N.A. Tahir, A. Tauschwitz, S. Udrea, D. Varentsov, K. Weyrich, Y. Maron, Laser Part. Beams **23**, 47–53 (2005)
11. Q. Wu, W.H. Zhu, H.M. Xiao, J. Mol. Model. **19**, 4039–4047 (2013)
12. S.J. Clark, M.D. Segall, C.J. Pickard, P.J. Hasnip, M.J. Probert, K. Refson, M.C. Payne, Z. Kristallogr. **220**, 567–570 (2005)
13. J.P. Perdew, K. Burke, M. Ernzerhof, Phys. Rev. Lett. **77**, 3865–3868 (1996)
14. A. Tkatchenko, M. Scheffler, Phys. Rev. Lett. **102**, 073005 (2009)
15. F. Birch, J. Geophys. Res. **83**, 1257 (1978)
16. Z.J. Wu, E.J. Zhao, H.P. Xiang, X.F. Hao, X.J. Liu, J. Meng, Phys. Rev. B **76**, 054115 (2007)
17. G.V. Sin'ko, N.A. Smirnov, J. Phys. Condens. Matter **16**, 8101–8104 (2004)
18. G.V. Sin'ko, N.A. Smirnov, J. Phys.: Condens. Matter **14**, 6989–7005 (2002)
19. W. Voigt, *Lehrbuch der kristallphysik* (Teubner, Leipzig, 1928)
20. A. Reuss, Z. Angew. Math. Mech. **9**, 49–58 (1929)
21. R. Hill, Proc. Phys. Soc. Lond **65**, 349–354 (1952)
22. S.F. Pugh, Philos. Mag. **45**, 823–843 (1954)
23. S.X. Cui, D.Q. Wei, H.Q. Hu, Z.Z. Gong, J. Appl. Phys. **113**, 083516 (2013)
24. W.H. Zhu, H.M. Xiao, Struct. Chem. **21**, 657 (2010)